Journal of Colloid and Interface Science 550 (2019) 180–189

Contents lists available at ScienceDirect

Journal of Colloid and Interface Science

journal homepage: www.elsevier.com/locate/jcis

Regular Article

Electrospun CuO-ZnO nanohybrid: Tuning the nanostructure for improved amperometric detection of hydrogen peroxide as a non-enzymatic sensor

Sahar Daemi [a], Shahram Ghasemi [b], Ali Akbar Ashkarran [c,*]

[a] Department of Physics, Faculty of Basic Sciences, University of Mazandaran, Babolsar, Iran
[b] Faculty of Chemistry, University of Mazandaran, Babolsar, Iran
[c] Department of Chemistry and Chemical Biology, Harvard University, 12 Oxford Street, Cambridge, MA 02138, USA

GRAPHICAL ABSTRACT

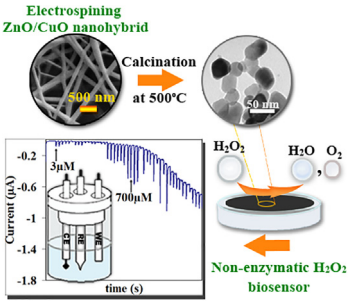

ARTICLE INFO

Article history:
Received 16 February 2019
Revised 20 April 2019
Accepted 29 April 2019
Available online 30 April 2019

Keywords:
Electrospinning
ZnO-CuO nanofibers
Hydrogen peroxide
Non-enzymatic sensor
Amperometry

ABSTRACT

Hydrogen peroxide (H_2O_2) is a by-product of some biochemical processes which is catalyzed by enzymes such as glucose oxidase (GOx), cholesterol oxidase (ChoOx), etc and its overproduction in living cells can trigger cancer growth and various diseases. Therefore, H_2O_2 sensing is of great importance in the determination of diseases as well as industries and environmental health plans. We produced ZnO-CuO nanofibers by electrospinning method for non-enzymatic electrochemical H_2O_2 sensing. The sensing properties of the carbon paste electrode (CPE) modified with ZnO (0.3 wt%)/CuO (0.7 wt%) nanofibers (named as ZnO3-CuO7) for detection of H_2O_2 were explored in phosphate-buffered saline (PBS) at pH ~ 7.4 solution. The ZnO3-CuO7 nanofiber exhibited the lowest charge transfer resistance and the highest electrocatalytic performance among other modified electrodes for detection of H_2O_2 and considered as an optimized sample. The effect of scan rate and H_2O_2 concentration in the reduction process were also investigated by cyclic voltammetry (CV) and the mechanism for the electrochemical reaction of H_2O_2 at the surface of the optimized electrode was studied. The diffusion coefficient of H_2O_2 and the catalytic rate constant were evaluated by chronoamperometry as 1.65×10^{-5} cm^2 s^{-1} and 6×10^3 - cm^3 mol^{-1} s^{-1}, respectively. Furthermore, amperometric detection of H_2O_2 with a low detection limit of 2.4 μM and a wide linear range of 3 to 530 μM were obtained. Meanwhile, the optimized electrode displayed no recognizable response towards some biomolecules such as ascorbic acid, uric acid, dopamine and glucose. The obtained results confirmed that the modified electrode shows high sensitivity and selectivity as a H_2O_2 biosensor with improved reproducibility and stability.

* Corresponding author.
E-mail address: ashkarran@fas.harvard.edu (A. Akbar Ashkarran).

https://doi.org/10.1016/j.jcis.2019.04.091
0021-9797/

1. Introduction

Fabricating one-dimensional metal oxide nanostructures with an uniform diameter and highly stable crystal structure through a cost-effective method is a promising challenge. One-dimensional structures provide an efficient platform to increase electrical conductivity, surface-to-volume area and catalytic performance [1,2]. Electrospinning method can produce nanofibers with desired dimensions at the nanometer scale with the aid of a polymeric gel containing metal precursors [3,4]. Controlling the physicochemical properties of the nanofibers such as diameter, length and morphology of hybrid metal oxides is of significant interest and the electrospinning technique can be considered as one of the most efficient ways of fabricating one-dimensional morphologies at the industrial level [5]. Metal oxides in various shapes, sizes and compositions are appropriate alternatives utilized in photoelectrochemical cells (PECs) [6], solar cells [7], Li-ion batteries [8] and sensors [9]. On the other hand, the coupling of two metal oxide semiconductors of p and n types not only separate charge carriers to make a heterojunction but also enhance the stability and catalytic activity. ZnO is a low-cost inorganic compound with wide band gap (3.37 eV), high mobility and non-toxicity. It is considered as a n-type semiconductor, but suffers from weak cycling performance as an electrode modifier [10]. CuO is an available and stable p-type semiconductor with narrow band gap (1.2 to 1.9 eV), which can be used in combination with ZnO as a hybrid nanostructure to enhance the electrochemical sensing properties due to the synergetic effects of binary metal oxides [11]. Besides, the CuO-ZnO p-n junction can offer more active sites, higher stability and faster electron transfer kinetics between electrode/electrolyte interface compared to the individuals [12,13].

Since hydrogen peroxide is an essential intermediate in biological and industrial systems, its non-enzymatic determination is of great importance [14]. A wide range of applications such as monitoring the H_2O_2 release from cancer cells and detecting the residual H_2O_2 level in food and water supplies is desirable [15,16]. Numerous methods such as chemiluminescence [17], oxidimetry [18] and titrimetry [19] have been developed for detection of H_2O_2 and most of these methods involve expensive and time-consuming procedures. On the other hand, although enzyme-based electrochemical sensors are highly sensitive to low concentrations of H_2O_2, they have some drawbacks of instability, high cost and complexity of the electrode fabrication. A wide range of transition metal oxides has been used as a mediator for non-enzymatic electrochemical sensing of H_2O_2. Among them, CuO and ZnO nanostructures are promising alternatives that have been explored in diversified morphologies for detection of H_2O_2 [20,21]. Many methods have been employed to fabricate CuO-ZnO composite such as thermal chemical vapor deposition (TCVD) [22], hydrothermal growth [23], solid-state grinding [24], electrodeposition [25], thermal oxidation [26] and high energy ball milling (HEBM) method [27]. However, a few reports are available to investigate the effect of various proportions of metal oxides using the electrospinning method [28,29].

Moreover, it is challenging to use the desired proportion of metal oxides for fabricating coupled CuO-ZnO heterojunction nanostructure to have the highest response to H_2O_2 in the biological environment. Here in, we have reported an amperometric H_2O_2 sensor based on CuO-ZnO electrospun nanocomposite as a transducer in PBS (pH = 7.4) medium. The structure, composition and proportion of various metal oxides were studied and the most efficient nanofiber for H_2O_2 determination was found. The limit of detection (LOD), diffusion coefficient and the catalytic rate constant of H_2O_2 were evaluated, which indicates that the electrospun CuO-ZnO nanofibers offer an excellent platform to fabricate H_2O_2 non-enzymatic biosensor.

2. Experimental details

2.1. Materials

Zinc acetate ($Zn(CH_3COO)_2{\cdot}2H_2O$), >99%, Merck), copper acetate ($Cu(CH_3COO)_2{\cdot}H_2O$), >99%, Merck), Triton X-100 (>99%, Merck), NaH_2PO_4 (>99%, Merck), Na_2HPO_4 (>99%, Merck), hydrogen peroxide (H_2O_2, 30 wt%) and ethanol (>99.9%, Merck) were used for experiments as received. Polyvinyl alcohol (PVA, M_w = 100000) was provided from Fluka to make a polymeric gel for electrospinning. $K_4[Fe(CN)_6]$ (>99%, Merck), $K_3[Fe(CN)_6]$ (>99%, Merck) and KCl (>99%, Merck) were used for the electrochemical impedance measurements. A mixture of graphite powder (particle diameter of 0.1 mm, Merck) and paraffin oil (density of 0.86 g cm^{-3}, Merck) was employed as a paste to fabricate a working electrode. For potential applications in biological environments, 0.1 M concentration of PBS in pH ~ 7.4 was used as supporting electrolyte. Na_2HPO_4 and NaH_2PO_4 were utilized to make 0.1 M PBS solution. All the chemicals were used as received and all the solutions were made with deionized (DI) water (Millipore water purification system, Direct-Q-3).

2.2. Characterizations

Scanning electron microscopy (SEM, KYKY-EM3200, from 10 to 26 keV accelerating energy) was used to evaluate morphology and the average diameter of the nanostructures and transmission electron microscopy (TEM, Philips EM208S instrument, from 80 to 100 keV accelerating energy) was performed for complementary analysis of size and shape of the nanostructures by deposition of nanostructures onto the copper grid at room temperature. The Energy-dispersive X-ray (EDX) and X-ray map (X-map) microanalyses determined the elemental composition of the nanostructures which were carried out by MIRA3 TESCAN-XMU at 5 to 20 keV accelerating energy. The X-ray diffraction analysis (XRD, Advance Brucker-8D instrument) was used to analyze the crystalline structure of the nanofibers using Cu K_α radiation source (λ = 0.15406 nm) in the 2θ ranging from 10° to 80°. In order to probe the molecular structure of samples, especially the metal oxides, Fourier-transform infrared spectroscopy (FTIR) (Bruker-Vector 22) was applied in the range of 400 to 4000 cm^{-1} by making KBr pellet. Ultraviolet–visible spectroscopy (UV–vis) was also conducted by a double beam Optizen POP spectrophotometer (Mecasys Company, Korea) from 200 to 1000 nm wavelengths to characterize the optical properties of nanofibers. The electrochemical tests were collected by a potentiostat/galvanostat AUTOLAB (Nova software model PGSTAT 302 N, Metrohm, Netherlands) coupled with a personal computer. The experiments were performed in a three-electrode cell containing a modified CPE, an Ag|AgCl (saturated KCl) electrode and a Pt wire as the working, reference and counter electrodes, respectively. The Electrochemical Impedance Spectroscopy (EIS) was utilized to compare the electrochemical performance of variously modified electrodes. The impedance spectra were measured using frequency response analyzer Palmsense (PSTrace software version 4.2.2, Netherlands) with AC voltage under open circuit potential, a signal amplitude of 10 mV and frequencies ranging from 1 to 100 KHz.

2.3. Synthesis of ZnO-CuO nanofibers

In order to prepare the polymeric gel for electrospinning, PVA aqueous solution of 7.3 wt% was prepared by gradual dissolving a proper amount of PVA powder in 80 °C water and then cooling to room temperature. A negligible amount of Triton X-100 as a surfactant was added to the PVA aqueous solution to decrease surface

tension and prevent bead formation in the final nanofibers. Then, an arbitrary proportion of metal acetates (total of 5 wt%) was added gently under magnetic stirring for 12 h, until the final polymeric gel was obtained. The as-prepared polymeric gel was loaded into a plastic syringe with a steel needle. The electrospinning process was conducted at room temperature using a home-made set up including a high-voltage DC power supply, a syringe pump (Ascor AP22) and an aluminum collector, which stands in a vertical position. The applied voltage between the needle of syringe and collector was fixed to 17 kV at a distance of 15 cm and the flow rate was fixed to 1 ml/h. The electrospun nanofibers were collected from the aluminum foil and calcined in an electrical furnace in the ambient air at 500 °C for 5 h to crystallize the nanostructure and remove the polymeric template of the nanofibers. Various nanofibers with a selective proportion of zinc acetate to copper acetate were synthesized to compare the electrochemical activity. For this purpose, nanofibers with zinc acetate to copper acetate weight ratio of 100:0, 70:30, 50:50, 30:70 and 0:100 (w/w %) were named as ZnO, ZnO7-CuO3, ZnO5-CuO5, ZnO3-CuO7 and CuO nanofibers, respectively.

2.4. Working electrode preparation

In a typical fabrication of working electrode, ZnO3-CuO7 nanofibers modified CPE (ZnO3-CuO7/CPE) was prepared by mixing a selective ratio of 20:50:30 (w/w %) for ZnO3-CuO7 nanofibers, graphite powder and paraffin oil to make a homogeneous paste. Then a glass tube with an internal diameter of 3.4 mm was used as a container of modified carbon paste with copper wire as an electrical connection. The prepared working electrode can be refreshed after each electrochemical measurement easily through smoothing the surface on a clean white paper and potential cycling in 0.1 M PBS (pH = 7.4) until a reproducible electrochemical behavior obtained. Other modified electrodes were fabricated by the method mentioned except the unmodified CPE that was prepared by mixing a 70:30 (w/w %) ratio of graphite powder to paraffin oil for comparison. A schematic representation of the fabrication method and electrode preparation for sensing process is depicted in Scheme 1.

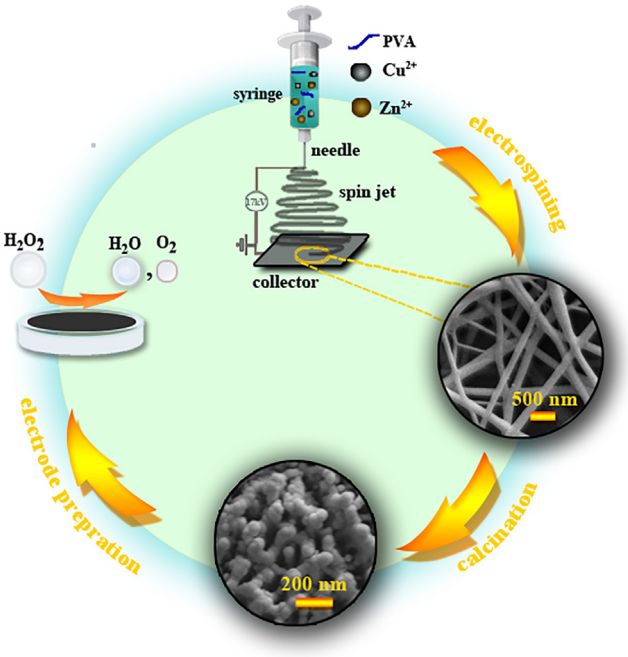

Scheme 1. Schematic illustration for fabrication of the metal oxide nanofibers by electrospinning method, the electrode preparation and the sensing process.

3. Results and discussion

3.1. Characterization of ZnO-CuO nanofibers

In the electrospinning method, the polymeric gel was exposed to a high-voltage in a relatively small distance to make a spinning jet out of the steel needle. PVA as a common and non-toxic organic material plays a vital role to bind the precursors and make the final nanofiber template [30]. After the calcination process, the cover pattern which is predominantly made of PVA, vanishes and various rough shapes appear. Fig. 1a, 1c and 1d exhibit the SEM images of CuO, ZnO7-CuO3 and ZnO nanofibers after calcination respectively, to show their structural morphology including their diameter distribution diagrams (measured by image processing software of Digimizer, MedCalc software). It was observed that even after the calcination process, the ZnO-containing nanofibers show smoother surface than CuO nanofibers. Fig. 1a represents CuO nanofibers with a diameter ranging from 60 to 200 nm and an average of 136 nm, which shows that some nanoparticles are embedded in the nanofiber structure, while ZnO nanofibers (Fig. 1d) introduce interwoven web nanostructures with a diameter ranging from 150 to 450 nm and an average of 249 nm. Fig. 1c demonstrates that the mean diameter of binary metal oxide such as ZnO7-CuO3 nanofibers decreased compared to bare CuO and ZnO nanofibers, ranging from 25 to 375 nm with an average of 125 nm. Fig. 1b and 1e illustrate the elemental analysis of CuO and ZnO nanofibers by X-map analysis. It is apparent that the Cu and Zn have been oxidized successfully and uniform distribution of Zn, Cu and O atoms in the nanostructures is formed. Figs. S1 and S2 of supplementary information (SI) show the corresponding EDX spectrums which reveal no C peak in the spectrum and verify complete removal of PVA molecules in the final nanofiber structure. Fig. 1f and g display ZnO3-CuO7 nanofibers and their corresponding diameter histograms before and after the calcination process. The as-electrospun nanofibers have an approximately uniform shape with a diameter ranging from 40 to 215 nm with an average of 126 nm (Fig. 1f). Indeed, the introduction of Triton X-100 as a surfactant in the initial polymeric gel can not only improve the stability of the spinning jet but also eliminate beads effectively via suppressing the surface tension of nanofibers and thus the creation of uniform nanofibers [31]. However, Fig. 1g shows that nanofibers are formed of chain-like nanoparticles after the calcination process and the diameter decreased to values between 40 and 110 nm with an average of 70 nm. Comparing the result of Fig. 1g with c reveals that the average diameter of nanofibers decreased in the presence of CuO as a major proportion and the nanofibers turned to a chain of nanoparticles. The X-map analysis of ZnO3-CuO7 nanofibers which is depicted in Fig. 1h also demonstrates a uniform dispersion of Zn, Cu and O elements. Moreover, Fig. S3 shows the EDX spectra of ZnO3-CuO7 nanofibers which confirm the presence of both Zn (60.0 wt%) and Cu (31.2 wt%) elements with 8.6 wt% of oxygen in the final nanostructure. TEM analysis provides more insights into the specific details of the nanostructures and enables more precise size measurements. Fig. 1i represents a typical TEM image of ZnO3-CuO7 nanofibers after calcination, which indicates that after calcination the nanofiber template vanishes and some interconnected nanoparticles with an average diameter of 35 nm appears.

Fig. 2a represents the absorbance spectra of nanofibers by UV–vis spectroscopy to investigate the optical properties of nanofibers. The obtained results revealed that ZnO nanofibers have strong and sharp absorption at 370 nm while CuO nanofibers have a broad absorption peak in the wide region of visible light around 800 nm. However, ZnO3-CuO7 nanofibers demonstrated both

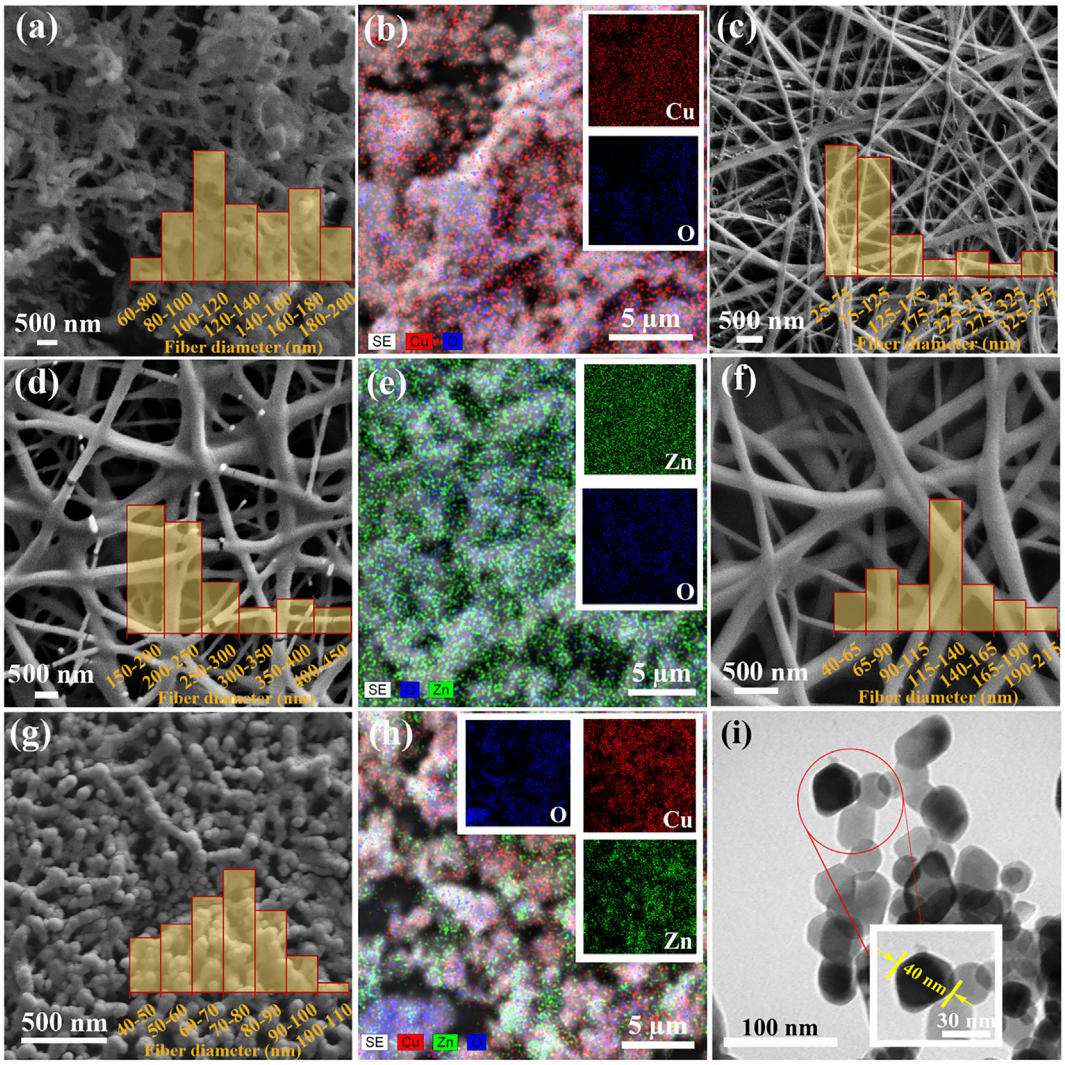

Fig. 1. Typical (a) SEM images and (b) the corresponding X-map of CuO, (c) SEM images of ZnO7-CuO3, (d) SEM images and (e) the corresponding X-map of ZnO nanofibers after calcination process, Typical SEM images of ZnO3-CuO7 nanofibers (f) before and (g) after calcination process (the insets are the corresponding diameter histograms) with the (h) corresponding X-map and (i) Typical TEM images of ZnO3-CuO7 nanofibers after calcination process.

characteristic peaks, one at 380 nm with a slight red shift compared to ZnO nanofibers and another wide absorption peak at around 750 nm with a small blue shift compared to CuO nanofibers [6]. This phenomenon indicates the integration of two semiconductors due to the band alignment of the p-n junction. Moreover, the appearance of two characteristic peaks in the absorption spectrum of ZnO3-CuO7 nanofibers demonstrates that they are composed of many n-type ZnO and p-type CuO nanograins in contact with each other creating ZnO3-CuO7 nanocomposite [32]. The FTIR spectra were also employed to evaluate the vibrational modes of calcined and non-calcined nanofibers as a evidence of metal oxide formation and also the removal of organic components such as PVA molecules in the calcined ZnO3-CuO7 nanofibers (Fig. 2b). Fig. 2b(i) exhibits the FTIR spectra of non-calcined ZnO3-CuO7 nanofibers, where the peaks at 2920, 1726, 1583 and 1430 cm^{-1} are attributed to C—H, C═O, C═C stretching and CH_2 (C—H bending vibration of CH_2) vibrations of PVA molecules, respectively [33]. The broad peak at nearly 3400 cm^{-1} corresponds to the adsorbed water molecules on the non-calcined ZnO3-CuO7 nanofibers. After the calcination process at 500 °C in Fig. 2b(j) the characteristic peaks related to the PVA molecule were suppressed or vanished approximately, while new peaks emerged at 437 and 501 cm^{-1} assigned to Zn–O and Cu–O stretching vibrations. Fig. 2b(k) and 2b(l) represent FTIR spectrums of calcined ZnO and CuO nanofibers, respectively, which confirm the formation of metal oxide similar to calcined ZnO3-CuO7 nanofibers. The peaks at 474 and 513 cm^{-1} are assigned to Zn–O and Cu–O stretching vibrations with an inconsiderable shift compared to calcined ZnO3-CuO7 nanofibers.

Previous reports denoted that at calcination temperatures above 300 °C nanofibers contain mixed crystalline phases of CuO and Cu_2O with a dominating phase of CuO, while at the temperature of 500 °C the pure crystalline CuO phase appears [34]. Furthermore, the thermal behavior of the as-prepared nanofibers also revealed that degradation of PVA molecule and acetate groups is accomplished at 500 °C. Therefore, the calcination process was carried out at 500 °C and the crystal structure and phase composition of nanofibers were identified by XRD analysis which is illustrated in Fig. 2c. The XRD patterns of ZnO, CuO and ZnO3-CuO7 nanofibers exhibited sharp diffraction peaks with high intensity which confirm the great crystalline feature and removal of polymer molecules in the nanofibers after calcination process. The peaks of CuO nanofibers, appeared at $2\theta = 32.64°$, 35.6°, 38.8°, 46.56°, 48.88°, 53.6°, 58.32°, 61.68°, 66.4°, 68.2°, 72.68° and 75.36, can be assigned to (1 1 0), (0 0 2), (1 1 1), (−1 1 2), (−2 0 2), (0 2 0), (2 0 2), (1 1 3),

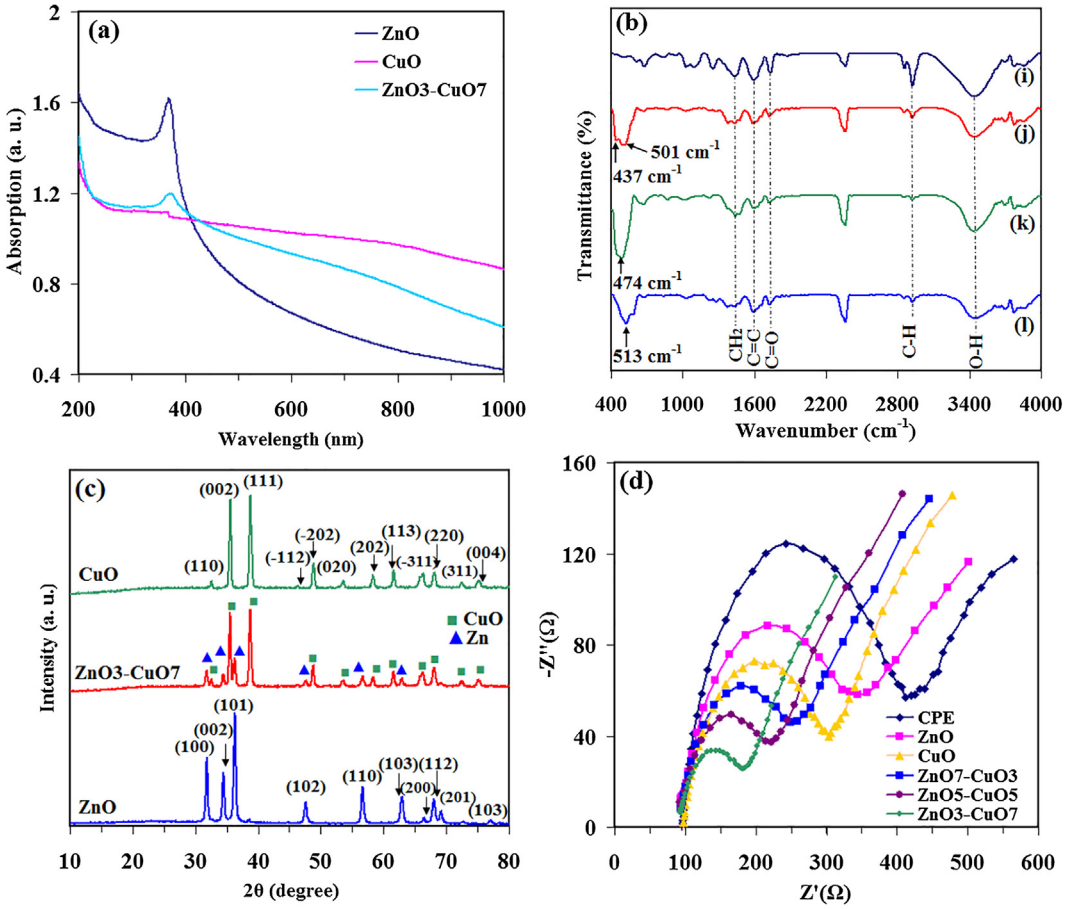

Fig. 2. (a) UV–vis absorption spectrum of ZnO, CuO and ZnO3-CuO7 nanofibers, (b) FT-IR spectra of ZnO3-CuO7 nanofibers (i) before and (j) after calcination, (k) ZnO nanofibers and (l) CuO nanofibers, (c) XRD patterns of CuO, ZnO and ZnO3-CuO7 and (d) EIS of the bare CPE, ZnO, CuO, ZnO7- CuO3, ZnO5-CuO5 and ZnO3-CuO7 nanofiber electrodes in 5 Mm $[Fe(CN)_6]^{3-/4-}$ solution containing 0.1 M KCl.

(−3 1 1), (2 2 0), (3 1 1) and (0 0 4) planes of tenorite (monoclinic) crystal structure (JCPDS card No. 05–0661), respectively. No other impurity peaks related to Cu_2O phase were identified, that approve the pure CuO crystalline phase [35]. The peaks of ZnO nanofibers also detected at 2θ = 31.84°, 34.52°, 36.32°, 47.64°, 56.68°, 63°, 66.52°, 68.2°, 69.56° and 77.2° which are indexed as (1 0 0), (0 0 2), (1 0 1), (1 0 2), (1 1 0), (1 0 3), (2 0 0), (1 1 2), (2 0 1) and (1 0 3) planes of zincite (Hexagonal) crystal structure (JCPDS card No. 36–1451), respectively. The ZnO3-CuO7 nanofibers represent the diffraction peaks of both CuO and ZnO nanofibers, which denotes the co-existence of binary metal oxides, indicative of n-ZnO/p-CuO heterojunction [28]. As the evidence of PVA decomposition, there is no additional peak around 20° in all the nanofibers, which is related to the extinction of nanofiber's template [36]. The mean crystallite size of ZnO, CuO and ZnO3-CuO7 nanofibers by using Debye-Scherrer equation were found to be 22.29, 30.31 and 31.6 nm, respectively [37].

The EIS technique was employed to probe the interfacial changes in the resistance of variously modified electrodes. Fig. 2d shows the Nyquist plot of bare CPE, ZnO, CuO, ZnO7- CuO3, ZnO5-CuO5 and ZnO3-CuO7 nanofiber modified electrodes in the frequency range of 1 Hz to 100 kHz in 5 Mm $[Fe(CN)_6]^{3-/4-}$ solution containing 0.1 M KCl. All the EIS spectra represent a Nyquist plot with a semicircle at the high-frequency region and a linear plot at the low-frequency region. The semicircle at high frequencies signifies the resistance which originates from charge transfer limitation (R_{ct}) and the linear response at low frequencies is the evidence of Warburg resistance that demonstrates a diffusion-controlled process of electrolyte ions [24]. The bare CPE electrode illustrates a large semicircle diameter with R_{ct} ~400 Ω. The semicircle diameter of the other electrodes is smaller than the CPE electrode, which denotes the better charge transfer after electrode surface modification. Furthermore, the linear part of the Nyquist plot reveals the diffusion of ions to the surface of the electrodes. It can be seen that by increasing the weight ratio of the CuO in the final nanofiber structure the diameter of the semicircle decreases and the ZnO3-CuO7/CPE electrode shows the lowest amount of resistance (R_{ct} ~200 Ω) compared to other modified electrodes. Therefore, it can be concluded that the synergetic effect of ZnO and CuO improves the charge transfer at the surface of the electrode. In addition, the reduction of resistance may be related to the decrease in the nanostructure size and the better effectiveness of CuO in the conductivity of nanostructure [38,39].

The effective surface area of modified electrodes was also obtained with the $K_4Fe(CN)_6$ solution as a redox probe (Figure S4). The effective surface areas of bare CPE and ZnO3-CuO7/CPE were estimated as 0.101 cm^2 and 0.137 cm^2 which suggests that ZnO3-CuO7 nanofiber can increase the electrode active surface area and consequently the electrocatalytic ability.

3.2. Electrochemical properties of ZnO3-CuO7/CPE

The CV profiles of bare CPE and modified electrodes with nanofibers in 0.1 M PBS (pH = 7.4) in the absence and presence of H_2O_2 are demonstrated in Fig. 3a-b, respectively. In the absence of H_2O_2, CuO/CPE represents specified redox peak related to the oxidation

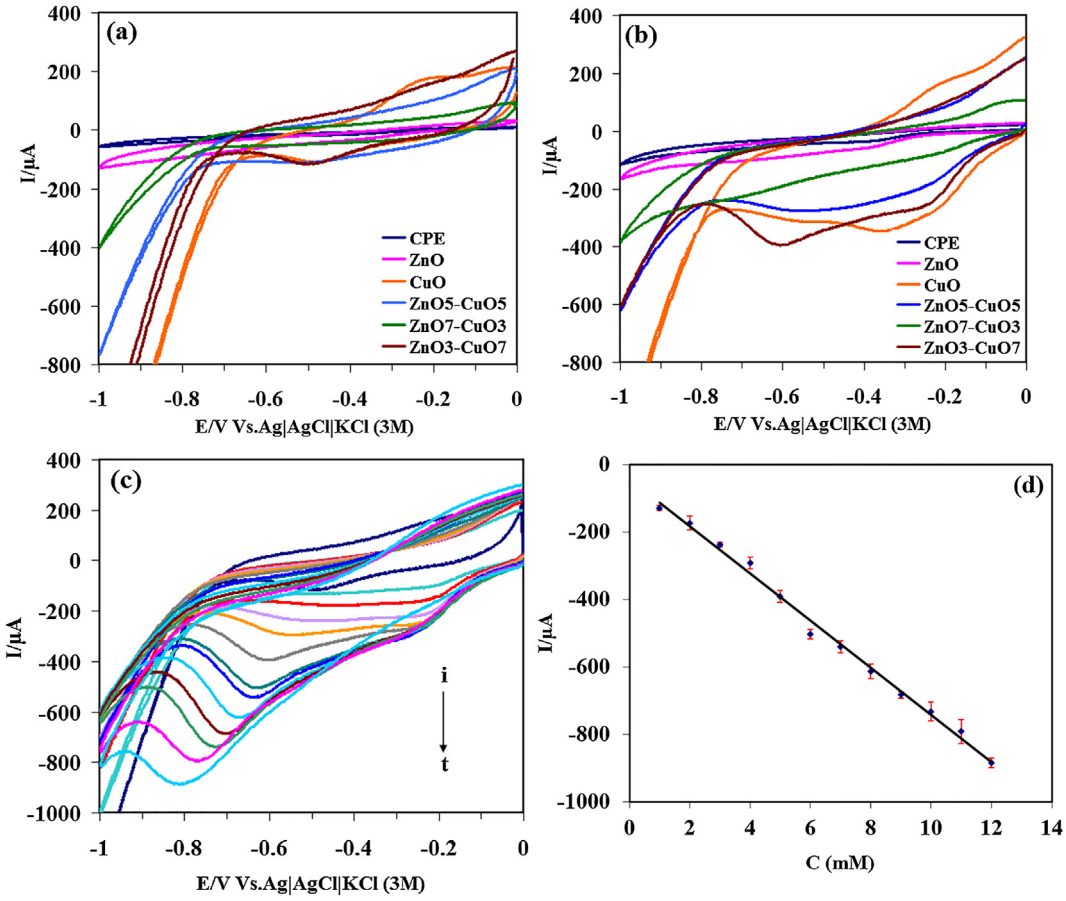

Fig. 3. The CVs of bare CPE, ZnO/CPE, CuO/CPE, ZnO5-CuO5/CPE, ZnO7-CuO3/CPE and ZnO3-CuO7/CPE at scan rate of 50 mV s^{-1} in 0.1 M PBS (pH = 7.4) solution (a) in the absence of H_2O_2 and (b) in the presence of 5 mM H_2O_2, (c) CVs of ZnO3-CuO7/CPE electrode in 0.1 M PBS solution (pH = 7.4) in the presence of various H_2O_2 concentrations: (i) 1, (j) 2, (k) 3, (l) 4, (m) 5, (n) 6, (o) 7, (p) 8, (q) 9, (r) 10, (s) 11 and (t) 12 mM and (d) the corresponding calibration plot of I_{pc} vs H_2O_2 concentration.

and reduction of Cu species (an anodic peak at −0.2 V and a cathodic peak is at −0.5 V). Whereas, ZnO/CPE do not show any oxidation and reduction peak, which suggest that CuO undergoes redox process through Cu(II)/Cu(I) conversion. In the presence of H_2O_2 the current value increased significantly for all the modified electrodes. ZnO/CPE shows no cathodic peak of current in the presence of 5 mM H_2O_2, while ZnO3-CuO7/CPE represents the highest value of reduction peak current at potential of −0.6 V. The results confirm that higher concentration of CuO in the modified electrodes enhances the catalytic activity and the mechanism of H_2O_2 reduction is based on the catalytic role of CuO in the reaction process. First, the Cu(II) is reduced to Cu(I) while H_2O_2 is reduced to O_2 and H_2O simultaneously. Then the catalyst is regenerated which facilitate the electron transfer to H_2O_2. Therefore, the optimized ZnO3-CuO7/CPE was selected for further electrochemical studies toward H_2O_2 determination. On the other hand, ZnO3-CuO7 nanofibers show a rough surface with lots of nanograins which could improve the current response. In fact, the ZnO3-CuO7 composite nanofibers with small-sized nanograins probably contain a large number of p-n junctions that could increase the sensing properties at its surface [40].

Furthermore, the effect of analyte concentration has been investigated in Fig. 3c-d. The error bars are the standard deviation of the mean value extracted from 3 distinct measurements. It is apparent that in the presence of H_2O_2 an additional reduction peak appears in the CV curve which screens the cathodic peak of CuO to Cu_2O transition and linearly enhances with increasing H_2O_2 concentration in the range between 1 and 12 mM (Fig. 3d). This phenomenon can explain enhanced sensing efficiency of the CuO-contained modified electrodes and the effect of CuO-ZnO p-n junction with a specified weight ratio toward H_2O_2 reduction. By increasing H_2O_2 concentration the cathodic peak shifts to higher potentials which demonstrate the surface adsorption of the species and charge transfer limitation between H_2O_2 and electrode surface. In fact, the higher effective surface and better electron transfer at ZnO3-CuO7 modified electrode may cause the quantitative measurement of response current.

Fig. 4a depicts the effect of scan rate on the cathodic peak current resulting from H_2O_2 reduction. The cathodic peak is linearly proportional to the square root of scan rate from 10 to 600 mV s^{-1} in the presence of 4 mM H_2O_2 (Fig. 4b) which is related to the diffusion-controlled electrochemical process. Moreover, the reduction peak potential (E_p) shifted to the less positive potentials with the increase of scan rate which is ascribed to the kinetic limitation of H_2O_2 reduction. It should be noted that the experiment was repeated three times and the average values are reported. Fig. 4c displays a linear relation between E_p and log (v) signifying an irreversible reduction of H_2O_2. The value of transfer coefficient (α) for the irreversible process of H_2O_2 reduction is obtained from the following equation [41]:

$$E_p = [2.303RT/(1-\alpha)n_\alpha F]\log v + K \quad (1)$$

where R,T, F and K are constant values as mentioned in the literature. From the slope of E_p vs. log v plot, the value of α is obtained 0.61 for electroreduction of H_2O_2.

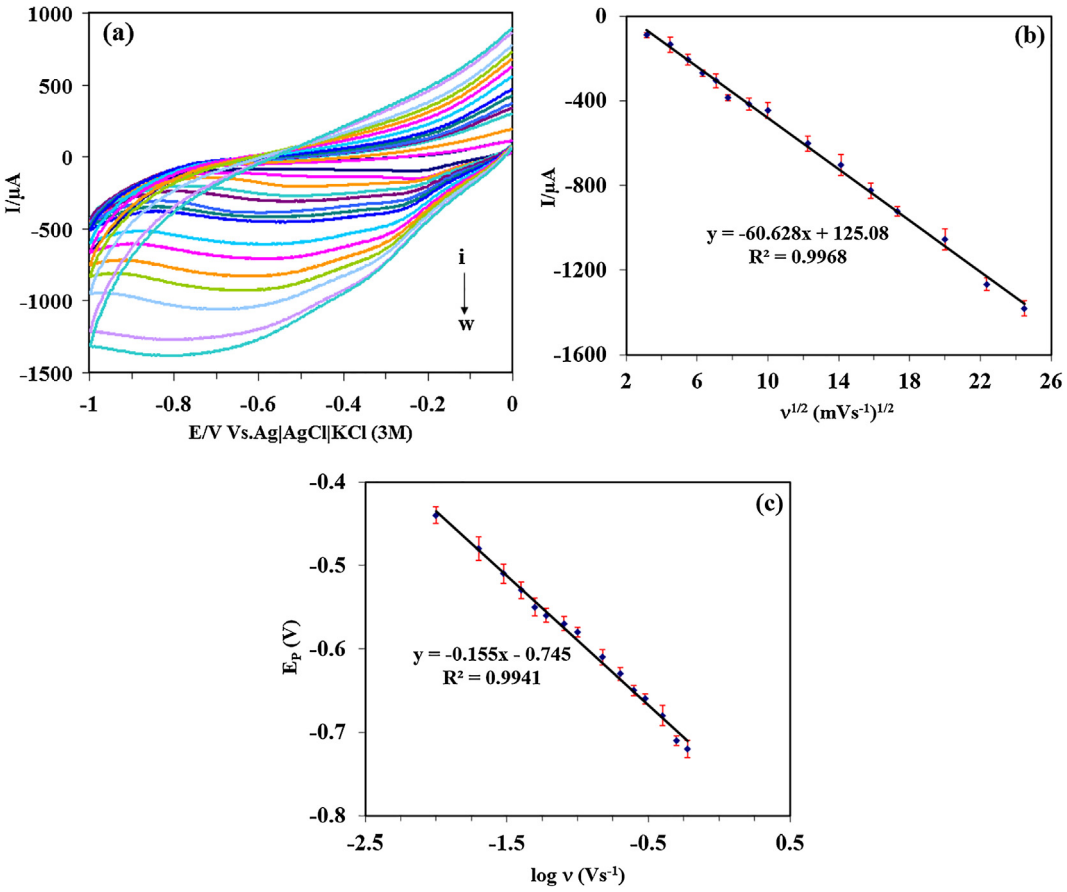

Fig. 4. (a) CVs of ZnO3-CuO7/CPE electrode in 0.1 M PBS (pH = 7.4) containing 4 mM H_2O_2 at different scan rates: (i) 10, (j) 20, (k) 30, (l) 40, (m) 50, (n) 60, (o) 80, (p) 100, (q) 150, (r) 200, (s) 250, (t) 300, (u) 400, (v) 500 and (w) 600 mV s^{-1}, (b) the plot of I_{pc} vs $\nu^{1/2}$ and (c) the plot of E_{pc} vs log ν.

3.3. Chronoamperometric studies

Chronoamperometry was employed to get more information about the reduction of H_2O_2 through the calculation of catalytic rate constant and diffusion coefficient of H_2O_2 at the surface of ZnO3-CuO7/CPE electrode. Figure S5a displays the chronoamperograms of ZnO3-CuO7/CPE in the absence and presence of different concentrations of H_2O_2 by setting the potential at −0.45 V vs. Ag|AgCl (KCl 3 M). The exponential dependence of I-t reveals that the H_2O_2 reduction process is diffusion-controlled which is described by Cottrell equation [42]. The cathodic current enhanced with increasing H_2O_2 concentration while H_2O_2 reduction generally occurs at the electrode/solution interface. Figure S5b demonstrates a linear plot of I vs. $t^{-1/2}$ for oxidation of H_2O_2 at ZnO3-CuO7/CPE electrode, which is described by [43]:

$$I = nFACD^{1/2}\pi^{-1/2}t^{-1/2} \quad (2)$$

where F is Faraday's constant, A is the geometrical surface area of the electrode, C is the bulk concentration of H_2O_2, t is time and D is the diffusion coefficient. From the linear slope of I vs. $t^{-1/2}$ the mean value of D is found to be 1.65×10^{-5} cm^2 s^{-1}.

Figure S5c exhibits a linear plot of I_C/I_L vs. $t^{1/2}$ which can be simulated by the simplified version of the equation reported before [44]:

$$I_C/I_L = \pi^{1/2}(kCt)^{1/2} \quad (3)$$

where k is the catalytic rate constant (cm^3 mol^{-1} s^{-1}), C is the bulk concentration of H_2O_2 (mol cm^{-3}), t is the time (s) and I_C and I_L are the catalytic currents of H_2O_2 and the limiting current in the absence of H_2O_2 at ZnO3-CuO7/CPE. From the linear interval of I_C/I_L versus $t^{1/2}$ for all concentrations, the mean value of k is evaluated as 6×10^3 cm^3 mol^{-1} s^{-1}.

3.4. Amperometric detection of H_2O_2

Amperometry is a more sensitive technique compared to CV which can be utilized to detect low concentrations of the analyte. In order to render the sensing properties of the as-prepared electrode, a typical current–time plot of ZnO3-CuO7/CPE was recorded with successive injection of H_2O_2 in the concentration ranging from 3 μM to 10.3 mM at a fixed potential of −0.45 V. As shown in Fig. 5a, upon each injection a rapid and stable amperometric response is observed. The modified electrode was used for 3 repeated amperometric measurements. Fig. 5b and 5c show the calibration plots with two linear dependence between the absolute value of current and H_2O_2 concentration from 3 to 530 μM and also from 530 μM to 10.3 mM with the sensitivity of 1.11 and 0.77 μA μM^{-1} cm^{-2}, respectively. The sensitivity declined in the second linear range of H_2O_2 concentration, denoting a mild electrode surface saturation by O_2 bubbles and make less electroactive sites available for electrochemical reactions, which is similar to the previous reports [45]. The LOD was evaluated as 2.4 μM when the signal-to-noise ratio was considered as 3. The analytical parameters of the ZnO3-CuO7/CPE electrode are comparable with other H_2O_2 sensors, especially with identical materials that are summarized in Table 1. The results confirmed that ZnO3-CuO7/CPE electrode provides a large surface area for H_2O_2 reduction which causes comparable LOD, overpotential and catalytic rate constant.

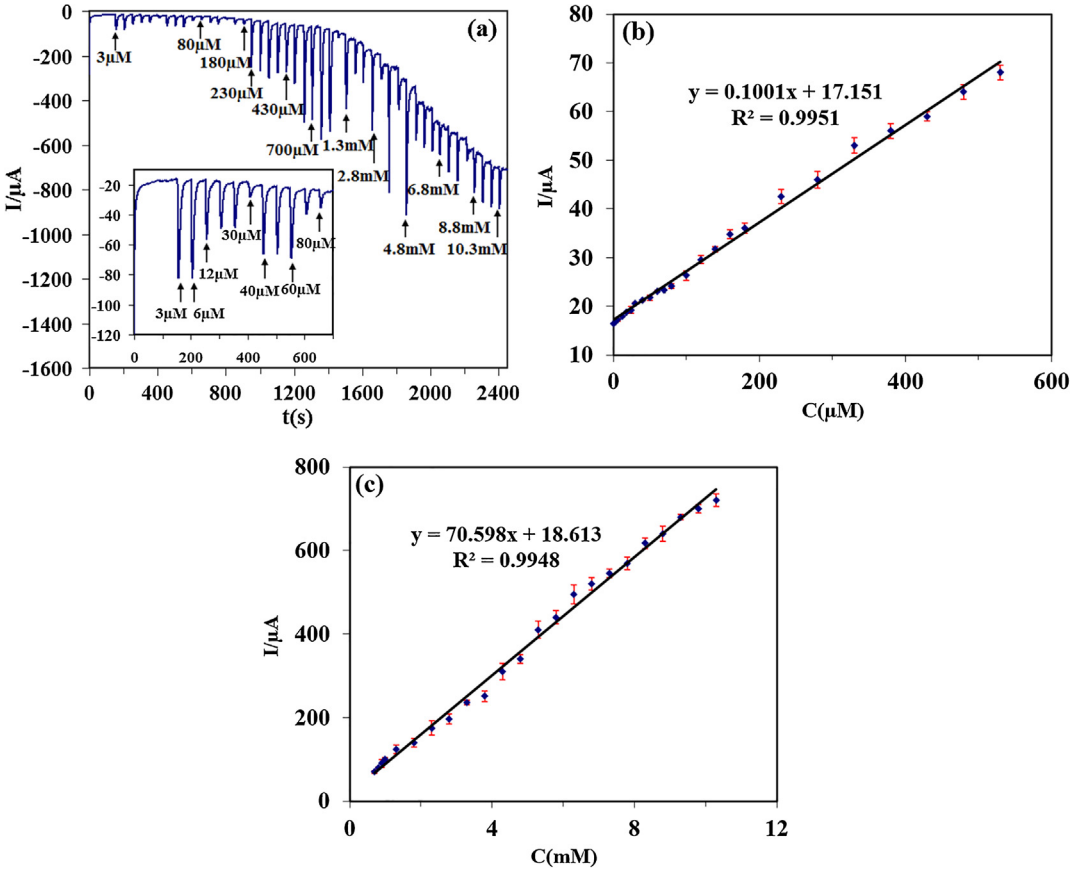

Fig. 5. (a) Amperometric response curve of ZnO3-CuO7/CPE to successive addition of H_2O_2 into 0.1 M PBS (pH = 7.4) at applied potential of −0.45 V (vs. Ag|AgCl), (b) the corresponding calibration plot in the range of 3 to 530 μM and (c) the calibration plot in the range of 530 μM to 10.3 mM.

3.5. Selectivity, stability and reproducibility

The selectivity of the as-prepared sensor was examined in Fig. 6a by adding a 20-fold concentration of potentially interfering biomolecules in the electrolyte such as G (glucose), UA (uric acid), AA (ascorbic acid) and DA (dopamine) during the amperometry test. The sensor detected a negligible interference compared with two successive injections of 0.1 mM H_2O_2 in the solution. It has been reported that the amperometric determination of H_2O_2 in the negative potentials may cause less interference in the results [44]. In each test, a refreshed electrode surface is cycled 10 times until an invariant plot is obtained. The stability of the modified electrode was studied through amperometric behavior of the electrode for a time duration of 1000 s at the potential of −0.45 V. As shown in Fig. 6b the blank signal remained almost constant during the entire test, confirming the stability of the sensor. Moreover, the storage stability of the modified electrode was investigated by CV in the presence of H_2O_2 after one month storing at room temperature. Surprisingly, the electrode restored up to nearly 90% of its initial response to H_2O_2 reduction. Also, the working stability of the electrode was examined by recording amperogram after injecting 0.1 mM H_2O_2 in the solution for a time duration of 2400 s (Fig. 6c). The current signal remained stable during the experiment without any distinguishing variation from the main response. The reproducibility of the sensor was tested for three ZnO3-CuO7/CPE electrodes fabricated independently with the same method. The CV was employed to detect a constant concentration of H_2O_2 and the relative standard deviation (RSD) was found to be 4.2% for the cathodic peak current. The results demonstrate that the modified electrode shows selectivity, stability and reproducibility for effective measurement of H_2O_2.

Table 1
Comparison of H_2O_2 electroanalytical performance at the surface of modified electrodes.

Electrode	Applied potential (V)	LOD (μM)	Sensitivity	Linear range (mM)	medium	Ref
CuO-SiNWs	−0.4	1.6	22.27 μA μM^{-1}	0.01–13.18	PBS (pH 7.0)	[46]
Cu_2O-rGO	−0.3	21.7	20.7 μA μM^{-1}	0.03–12.8	PBS (pH 7.4)	[47]
GNs/Nafion/AzI/AuNPs/GCE	−0.2	10	—	0.03–5	HAc–NaAc buffer (pH 4.0)	[48]
Cu_2O/GNs	−0.4	20.8	—	0.3–7.8	PBS (pH 7.4)	[49]
CuO-ZnO/FTO	−0.6	9.998	0.35686 μA μM^{-1}	0.01–1	PBS (pH 7.0)	[29]
MnO_2-MWCNTs	0.45	0.8	1.08 μA μM^{-1} cm^{-2}	0.0012–1.8	borate buffer (pH 7.8)	[50]
Co_3O_4/MWCNTs	−0.19	2.46	1.00 μA μM^{-1} cm^{-2}	0.02–0.43	NaOH 0.1 mol dm^{-3}	[44]
ZnO3-CuO7/CPE	−0.45	2.4	1.11 μA μM^{-1} cm^{-2}	0.003–0.53	PBS (pH 7.4)	This work

SiNW: Silicon Nanowire, rGO: reduced graphene oxide, GNs: Graphene Nanosheets, AzI: azure I, MWNT: multiwall carbon nanotube.

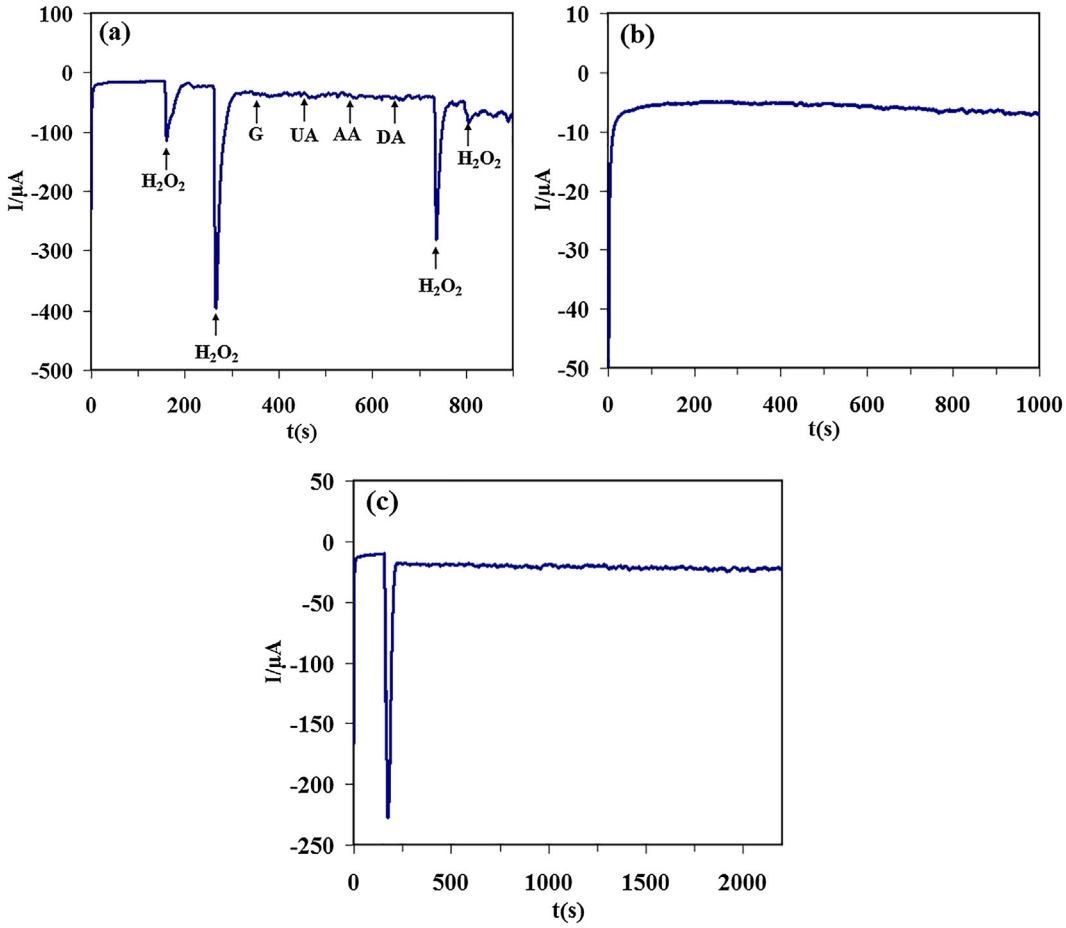

Fig. 6. (a) Amperometric response of ZnO3-CuO7/CPE for two successive addition of 0.1 mM H_2O_2 in the presence 2 mM of G, UA, AA and DA and the long-term stability of ZnO3-CuO7/CPE (b) in the absence of H_2O_2 and (c) upon injection of 0.1 mM H_2O_2 in the continuously stirred 0.1 M PBS at the applied potential of −0.45 V vs. Ag|AgCl.

4. Conclusions

In this study, ZnO/CuO nanofibers with various ratios of ZnO to CuO were fabricated through the electrospinning method, followed by calcination in air at 500 °C. Microscopic studies revealed that the ZnO3-CuO7 nanofibers have the lowest mean diameter among other nanostructures with a continuous nanoparticle appearance. The optical properties of the optimized nanofiber (ZnO3-CuO7) illustrated the presence of both absorption peaks of ZnO and CuO in the nanofiber which demonstrates the formation of the nanocomposite. The XRD analysis of the all synthesized nanofibers confirmed the formation of pure crystalline nanostructures of ZnO and CuO and the FTIR also revealed the complete degradation of organic compounds. Furthermore, the electrocatalytic performance of nanofibers modified CPE electrode for H_2O_2 reduction in PBS (pH = 7.4) was studied. It was found that the CPE modified with the optimized nanofiber (ZnO3-CuO7/CPE) represents the highest efficiency for H_2O_2 detection in a biological medium as well as the lowest charge transfer resistance according to the EIS measurements. At higher concentrations of CuO, the band narrowing occurs and the electrocatalytic properties of the nanofibers for detection of small molecules increased due to the rough shape and the presence of a large number of nanograins. In addition, the increased effective surface area of ZnO3-CuO7/CPE compared to unmodified electrode causes the better sensing performance of the nanocomposite. Therefore, the ZnO3-CuO7/CPE was utilized as an H_2O_2 biosensor with a sensitive amperometric response and lower detection limit of 2.4 μM compared to other similar nanomaterials. Moreover, the sensor exhibited wide linear range, high selectivity among other biomolecules, stability and reproducibility. Thus, the ZnO3-CuO7 based sensor possesses a promising potential as a non-enzymatic biosensor for biomedical devices in the future. Moreover, the optimized ZnO/CuO nanofiber can be utilized for sensing of other target analytes by tuning the concentration of metal oxides in the ZnO/CuO nanofibers.

Appendix A. Supplementary material

Supplementary data to this article can be found online at https://doi.org/10.1016/j.jcis.2019.04.091.

References

[1] G. Wu, X. Liang, L. Zhang, Z. Tang, M. Al-Mamun, H. Zhao, X. Su, Fabrication of highly stable metal oxide hollow nanospheres and their catalytic activity toward 4-nitrophenol reduction, ACS Appl. Mater. Inter. 9 (21) (2017) 18207–18214.
[2] Y. Xia, P. Yang, Y. Sun, Y. Wu, B. Mayers, B. Gates, Y. Yin, F. Kim, H. Yan, One-dimensional nanostructures: synthesis, characterization, and applications, Adv. Mater. 15 (5) (2003) 353–389.
[3] W.E. Teo, S. Ramakrishna, A review on electrospinning design and nanofibre assemblies, Nanotechnology 17 (14) (2006) R89.
[4] J. Su, G. Yang, C. Cheng, C. Huang, H. Xu, Q. Ke, Hierarchically structured TiO_2/PAN nanofibrous membranes for high-efficiency air filtration and toluene degradation, J. Colloid Interf. Sci. 507 (2017) 386–396.
[5] N. Horzum, R. Muñoz-Espí, G. Glasser, M.M. Demir, K. Landfester, D. Crespy, Hierarchically structured metal oxide/silica nanofibers by colloid electrospinning, ACS Appl. Mater. Inter. 4 (11) (2012) 6338–6345.
[6] U. Shaislamov, K. Krishnamoorthy, S.J. Kim, A. Abidov, B. Allabergenov, S. Kim, S. Choi, R. Suresh, W.M. Ahmed, H.-J. Lee, Highly stable hierarchical p-CuO/ZnO

nanorod/nanobranch photoelectrode for efficient solar energy conversion, Int. J. Hydrogen Energy 41 (4) (2016) 2253–2262.
[7] E. Palomares, J.N. Clifford, S.A. Haque, T. Lutz, J.R. Durrant, Control of charge recombination dynamics in dye sensitized solar cells by the use of conformally deposited metal oxide blocking layers, J. Am. Chem. Soc. 125 (2) (2003) 475–482.
[8] X. Chen, Y. Huang, X. Zhang, C. Li, J. Chen, K. Wang, Graphene supported ZnO/CuO flowers composites as anode materials for lithium ion batteries, Mater. Lett. 152 (2015) 181–184.
[9] H. Gao, Q. Yu, K. Chen, P. Sun, F. Liu, X. Yan, F. Liu, G. Lu, Ultrasensitive gas sensor based on hollow tungsten trioxide-nickel oxide (WO_3-NiO) nanoflowers for fast and selective xylene detection, J. Colloid Interf. Sci. 535 (2019) 458–468.
[10] L. Chen, J. Cui, X. Sheng, T. Xie, T. Xu, X. Feng, High-performance photoelectronic sensor using mesostructured ZnO Nanowires, ACS sens. 2 (11) (2017) 1567–1572.
[11] M.M. Rahman, A. Jamal, S.B. Khan, M. Faisal, CuO codoped ZnO based nanostructured materials for sensitive chemical sensor applications, ACS Appl. Mater. Inter. 3 (4) (2011) 1346–1351.
[12] S. Jung, K. Yong, Fabrication of CuO–ZnO nanowires on a stainless steel mesh for highly efficient photocatalytic applications, Chem. Commun. 47 (9) (2011) 2643–2645.
[13] S. Ghosh, D. Adak, R. Bhattacharyya, N. Mukherjee, ZnO/γ-Fe_2O_3 charge transfer interface toward highly selective h_2s sensing at a low operating temperature of 30° C, ACS sens. 2 (12) (2017) 1831–1838.
[14] K. Zhang, N. Zhang, H. Cai, C. Wang, A novel non-enzyme hydrogen peroxide sensor based on an electrode modified with carbon nanotube-wired CuO nanoflowers, Microchim. Acta 176 (1–2) (2012) 137–142.
[15] S. Kubendhiran, B. Thirumalraj, S.-M. Chen, C. Karuppiah, Electrochemical co-preparation of cobalt sulfide/reduced graphene oxide composite for electrocatalytic activity and determination of H_2O_2 in biological samples, J. Colloid Interf. Sci. 509 (2018) 153–162.
[16] J. Leong, Y. Seo, S.-H. Chu, C. Park, E.J. Jeon, S.-W. Cho, Y.Y. Yang, L.A. DiPietro, D. H. Kim, H. Kong, pore diameter of mesoporous silica modulates oxidation of H_2O_2-sensing chromophore in a porous matrix, Langmuir 34 (38) (2018) 11242–11252.
[17] S. Hanaoka, J. Lin, M. Yamada, Chemiluminescent flow sensor for hydrogen peroxide based on the decomposition of hydrogen peroxide catalyzed by cobalt (II)-ethanolamine complex immobilized on resin, Anal. Chim. Acta 426 (2001) 57–64.
[18] E. Hurdis, H. Romeyn, Accuracy of determination of hydrogen peroxide by cerate oxidimetry, Anal. Chem. 26 (2) (1954) 320–325.
[19] A. Brestovisky, E. KirowaEisner, J. Osteryoung, Direct and titrimetric determination of hydrogen peroxide by reverse pulse polarography, Anal. Chem. 55 (13) (1983) 2063–2066.
[20] Q. Rui, K. Komori, Y. Tian, H. Liu, Y. Luo, Y. Sakai, Electrochemical biosensor for the detection of H_2O_2 from living cancer cells based on ZnO nanosheets, Anal. Chim. Acta 670 (1–2) (2010) 57–62.
[21] M.A. Prathap, B. Kaur, R. Srivastava, Hydrothermal synthesis of CuO micro-/nanostructures and their applications in the oxidative degradation of methylene blue and non-enzymatic sensing of glucose/H_2O_2, J. Colloid Interf. Sci. 370 (1) (2012) 144–154.
[22] S. Pukird, W. Song, S. Noothongkaew, S.K. Kim, B.K. Min, S.J. Kim, K.W. Kim, S. Myung, K.-S. An, Synthesis and electrical characterization of vertically-aligned ZnO–CuO hybrid nanowire p–n junctions, Appl. Surf. Sci. 351 (2015) 546–549.
[23] R. Ahmad, N. Tripathy, M.-S. Ahn, K.S. Bhat, T. Mahmoudi, Y. Wang, J.-Y. Yoo, D.-W. Kwon, H.-Y. Yang, Y.-B. Hahn, Highly efficient non-enzymatic glucose sensor based on CuO modified vertically-grown ZnO nanorods on electrode, Sci. Rep. 7 (1) (2017) 5715.
[24] F. Wu, X. Wang, S. Hu, C. Hao, H. Gao, S. Zhou, Solid-state preparation of CuO/ZnO nanocomposites for functional supercapacitor electrodes and photocatalysts with enhanced photocatalytic properties, Int. J. Hydrogen Energy 42 (51) (2017) 30098–30108.
[25] U. Shaislamov, K. Krishnamoorthy, S.J. Kim, S. Choi, W. Chun, H.-J. Lee, Growth of CuO/ZnO nanobranched photoelectrode with enhanced stability for solar hydrogen generation, J. Nanosci. Nanotechnol. 16 (10) (2016) 10541–10547.
[26] X. Zhao, P. Wang, B. Li, CuO/ZnO core/shell heterostructure nanowire arrays: synthesis, optical property, and energy application, Chem. Commun. 46 (36) (2010) 6768–6770.
[27] A. Dhara, B. Show, A. Baral, S. Chabri, A. Sinha, N.R. Bandyopadhyay, N. Mukherjee, Core-shell CuO-ZnO pn heterojunction with high specific surface area for enhanced photoelectrochemical (PEC) energy conversion, Solar Energy 136 (2016) 327–332.
[28] A. Naseri, M. Samadi, N.M. Mahmoodi, A. Pourjavadi, H. Mehdipour, A.Z. Moshfegh, Tuning composition of electrospun ZnO/CuO nanofibers: toward controllable and efficient solar photocatalytic degradation of organic pollutants, J. Phys. Chem. C 121 (6) (2017) 3327–3338.
[29] S. Chabri, A. Dhara, B. Show, D. Adak, A. Sinha, N. Mukherjee, Mesoporous CuO–ZnO p–n heterojunction based nanocomposites with high specific surface area for enhanced photocatalysis and electrochemical sensing, Catal. Sci. Technol. 6 (9) (2016) 3238–3252.
[30] D. Malwal, P. Gopinath, Efficient adsorption and antibacterial properties of electrospun CuO-ZnO composite nanofibers for water remediation, J. Hazard. Mater. 321 (2017) 611–621.
[31] S.R. Hosseini, M. Kamali-Rousta, Preparation of electro-spun CuO nanoparticle and its application for hydrazine hydrate electro-oxidation, Electrochim. Acta 189 (2016) 45–53.
[32] B. Li, Y.J.S. Wang, Facile synthesis and photocatalytic activity of ZnO–CuO nanocomposite, Superlattices Microstruct. 47 (5) (2010) 615–623.
[33] C.L. Raju, J. Rao, B. Reddy, K.V. Brahmam, Thermal and IR studies on copper doped polyvinyl alcohol, B. Mater. Sci. 30 (3) (2007) 215–218.
[34] L.D.L.S. Valladares, D.H. Salinas, A.B. Dominguez, D.A. Najarro, S. Khondaker, T. Mitrelias, C. Barnes, J.A. Aguiar, Y. Majima, Crystallization and electrical resistivity of Cu_2O and CuO obtained by thermal oxidation of Cu thin films on SiO_2/Si substrates, Thin Solid Films 520 (20) (2012) 6368–6374.
[35] L. Cheng, Y. Tian, J. Zhang, Construction of pn heterojunction film of Cu_2O/α-Fe_2O_3 for efficiently photoelectrocatalytic degradation of oxytetracycline, J. Colloid Interf. Sci. 526 (2018) 470–479.
[36] Y. Nishio, R.J. Manley, Cellulose-poly (vinyl alcohol) blends prepared from solutions in N N-dimethylacetamide-lithium chloride, Macromolecules 21 (5) (1988) 1270–1277.
[37] U. Holzwarth, N. Gibson, The Scherrer equation versus the 'Debye-Scherrer equation', Nat. Nanotechnol. 6 (9) (2011) 534.
[38] L.-C. Jiang, W.-D. Zhang, A highly sensitive nonenzymatic glucose sensor based on CuO nanoparticles-modified carbon nanotube electrode, Biosens. Bioelectron. 25 (6) (2010) 1402–1407.
[39] Z. Amani-Beni, A. Nezamzadeh-Ejhieh, A novel non-enzymatic glucose sensor based on the modification of carbon paste electrode with CuO nanoflower: designing the experiments by response surface methodology (RSM), J. Colloid Interf. Sci. 504 (2017) 186–196.
[40] A. Katoch, S.-W. Choi, J.-H. Kim, J.H. Lee, J.-S. Lee, S.S.J.S. Kim, Importance of the nanograin size on the H_2S-sensing properties of ZnO–CuO composite nanofibers, Sensor. Actuat. B-Chem. 214 (2015) 111–116.
[41] S. Daemi, A.A. Ashkarran, A. Bahari, S. Ghasemi, Fabrication of a gold nanocage/graphene nanoscale platform for electrocatalytic detection of hydrazine, Sensor. Actuat. B-Chem. 245 (2017) 55–65.
[42] A. Ciszewski, G. Milczarek, Kinetics of electrocatalytic oxidation of formaldehyde on a nickel porphyrin-based glassy carbon electrode, J. Electroanal. Chem. 469 (1) (1999) 18–26.
[43] A.J. Bard, L.R. Faulkner, Electrochemical Methods, second ed., Wiley, New York, 2001.
[44] H. Heli, J. Pishahang, Cobalt oxide nanoparticles anchored to multiwalled carbon nanotubes: Synthesis and application for enhanced electrocatalytic reaction and highly sensitive nonenzymatic detection of hydrogen peroxide, Electrochim. Acta 123 (2014) 518–526.
[45] C. Cheng, Y. Huang, N. Wang, T. Jiang, S. Hu, B. Zheng, H. Yuan, D. Xiao, Facile fabrication of Mn_2O_3 nanoparticle-assembled hierarchical hollow spheres and their sensing for hydrogen peroxide, ACS Appl. Mater. Inter. 7 (18) (2015) 9526–9533.
[46] J. Huang, Y. Zhu, H. Zhong, X. Yang, C. Li, Dispersed CuO nanoparticles on a silicon nanowire for improved performance of nonenzymatic H_2O_2 detection, ACS Appl. Mater. Inter. 6 (10) (2014) 7055–7062.
[47] F. Xu, M. Deng, G. Li, S. Chen, L. Wang, Electrochemical behavior of cuprous oxide–reduced graphene oxide nanocomposites and their application in nonenzymatic hydrogen peroxide sensing, Electrochim. Acta 88 (2013) 59–65.
[48] Y. Zhang, Y. Liu, J. He, P. Pang, Y. Gao, Q. Hu, Electrochemical behavior of graphene/Nafion/Azure I/Au nanoparticles composites modified glass carbon electrode and its application as nonenzymatic hydrogen peroxide sensor, Electrochim. Acta 90 (2013) 550–555.
[49] M. Liu, R. Liu, W. Chen, Graphene wrapped Cu_2O nanocubes: non-enzymatic electrochemical sensors for the detection of glucose and hydrogen peroxide with enhanced stability, Biosens. Bioelectron. 45 (2013) 206–212.
[50] B. Xu, M.-L. Ye, Y.-X. Yu, W.-D. Zhang, A highly sensitive hydrogen peroxide amperometric sensor based on MnO_2-modified vertically aligned multiwalled carbon nanotubes, Anal. chim. acta 674 (1) (2010) 20–26.